

Lifting Transformer for 3D Human Pose Estimation in Video

Wenhai Li¹, Hong Liu¹, Runwei Ding¹, Mengyuan Liu², Pichao Wang³

¹Key Laboratory of Machine Perception, Shenzhen Graduate School, Peking University, China

²School of Intelligent Systems Engineering, Sun Yat-sen University, China

³Alibaba Group

{wenhaoli, hongliu, dingrunwei}@pku.edu.cn, nkliuyifang@gmail.com, pichao.wang@alibaba-inc.com

Abstract

Despite great progress in video-based 3D human pose estimation, it is still challenging to learn a discriminative single-pose representation from redundant sequences. To this end, we propose a novel Transformer-based architecture, called Lifting Transformer, for 3D human pose estimation to lift a sequence of 2D joint locations to a 3D pose. Specifically, a vanilla Transformer encoder (VTE) is adopted to model long-range dependencies of 2D pose sequences. To reduce redundancy of the sequence and aggregate information from local context, fully-connected layers in the feed-forward network of VTE are replaced with strided convolutions to progressively reduce the sequence length. The modified VTE is termed as strided Transformer encoder (STE) and it is built upon the outputs of VTE. STE not only significantly reduces the computation cost but also effectively aggregates information to a single-vector representation in a global and local fashion. Moreover, a full-to-single supervision scheme is employed at both the full sequence scale and single target frame scale, applying to the outputs of VTE and STE, respectively. This scheme imposes extra temporal smoothness constraints in conjunction with the single target frame supervision. The proposed architecture is evaluated on two challenging benchmark datasets, namely, Human3.6M and HumanEva-I, and achieves state-of-the-art results with much fewer parameters.

1. Introduction

3D human pose estimation aims to estimate 3D joint locations of a human body from images or videos, which is a regression problem. This task has drawn tremendous attention in the past decades [5, 19, 33, 47], with wide applications in computer animation [32], action understanding [24, 25, 42], and human-robot interactions [8, 10]. It is a challenging problem due to the depth ambiguity and self-occlusions.

Many state-of-the-art approaches adopt a two-stage

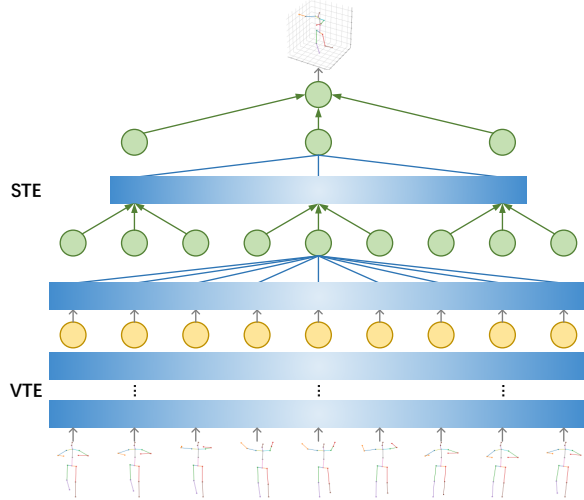


Figure 1. Our strided Transformer encoder (STE) takes the outputs of vanilla Transformer encoder (VTE) as input (yellow) and generates a 3D pose for the target frame as output (top). The self-attention mechanism (blue) concentrates on global context and strided convolution (green) aggregates information from local context.

pipeline [27, 31, 41], which first estimates 2D keypoints and then lifts them to the 3D space. Although the 2D-3D lifting methods benefit from the reliable performance of 2D pose detectors, it is still an ill-posed problem due to the depth ambiguity, where multiple 3D interpretations can map to the same 2D keypoints from monocular images. To resolve this ambiguity, some methods [1, 18, 34] exploit temporal information by leveraging past and future data in the sequence to predict the 3D pose of the target frame. For instance, Cai *et al.* [1] presented a local-to-global graph convolutional network to exploit spatial-temporal relations to estimate 3D poses from a sequence of skeletons. However, these approaches cannot explicitly and effectively model long-term dependencies result in small temporal receptive fields.

Vanilla Transformer [39] is developed for exploiting long-range dependencies and achieves tremendous success

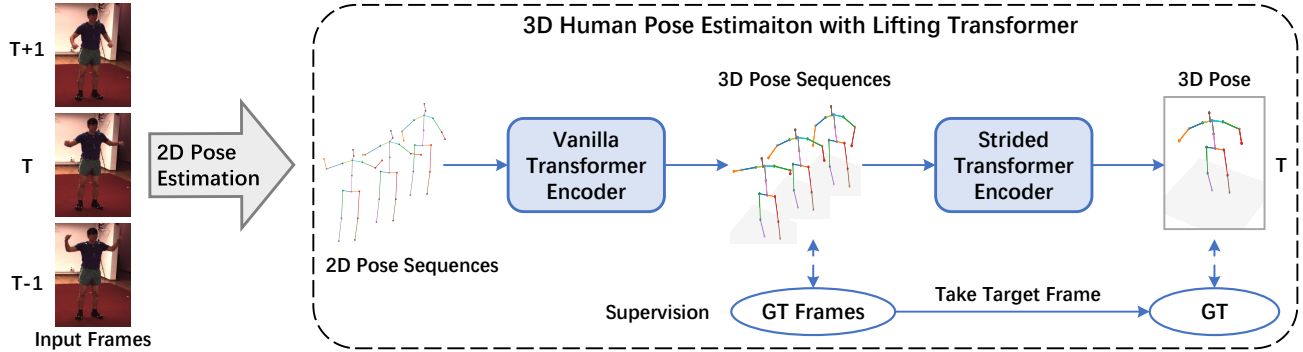


Figure 2. Overview of our proposed Lifting Transformer for predicting the 3D joint locations of the target frame from the estimated 2D pose sequences. The network first models long-range information via a vanilla Transformer encoder (VTE), and then aggregates the information to one target pose representation from the proposed strided Transformer encoder (STE). The model is trained end-to-end at both the full sequence scale and single target frame scale.

in natural language processing [37, 49] and computer vision [11, 12, 14, 20, 21]. It consists of self-attention module and point-wise feed-forward network (FFN). The self-attention module computes pairwise dot-product between all input elements to capture global-context information and the FFN acts as pattern detectors over the input across all layers [9]. Such design is a good choice for video-based 3D human pose estimation to capture long-range dependencies. However, the full-length representation in the vanilla Transformer encoder (VTE) [39] actually contains significant redundancy for video-based pose estimation, as nearby poses are quite similar. Based on the aforementioned observations, we propose to gradually merge nearby poses to reduce the sequence length till to one target pose representation. An alternative is to perform the pooling operation after the FFN [49]. However, lots of valuable information may be lost if using pooling operation and the local information can not be well exploited. Inspired by previous methods [26, 31] that take temporal convolutions to handle sequences with different input lengths, we propose to replace fully-connected layers in FFN with strided convolutions to progressively reduce the sequence length. The modified Transformer is dubbed strided Transformer encoder (STE), and it trades off the computation in FFN for constructing a deeper model and aggregates information in a global and local fashion to boost the model capacity, as shown in Figure 1. In addition, based on the outputs of VTE and STE, a novel full-to-single supervision scheme is proposed at both the full and single scales. More precisely, the full sequence scale can enforce temporal smoothness and single target frame scale helps learn a specific representation for the target frame.

The proposed architecture is called Lifting Transformer, as shown in Figure 2. Extensive experiments are conducted on two standard 3D human pose estimation datasets, i.e., Human3.6M [15] and HumanEva-I [35]. Experimental results show that our model achieves state-of-the-art performance.

mance.

We summarize our contributions as follows:

- We propose the Lifting Transformer, a Transformer-based architecture for 3D human pose estimation, which is simple and efficient to lift 2D joint locations to 3D poses.
- To reduce the sequence redundancy and computation cost, STE is introduced to progressively reduce the temporal dimensionality and aggregate information to a single-vector representation of pose sequences in a global and local fashion.
- A full-to-single supervision scheme is designed to impose extra temporal smoothness constraints during training at the full sequence scale and further refine the estimation at the single target frame scale.
- State-of-the-art results are achieved with fewer parameters on two commonly used benchmark datasets, making it a strong baseline for Transformer-based 3D pose estimation.

2. Related Work

One-stage pose estimation. At the early stage of applying deep neural networks on 3D pose estimation task, many methods [22, 30, 36, 46] learned the direct mapping from RGB images to 3D poses, termed as one-stage pose estimation. However, these methods require sophisticated architectures, which are impractical in realistic applications.

Two-stage pose estimation. Two-stage methods formulate the problem of 3D human pose estimation as 2D keypoint detection followed by 2D-3D lifting estimation [7, 27, 40]. For example, Martinez *et al.* [27] lifted 2D joint locations to 3D space via a fully-connected residual network. Fang *et al.* [7] proposed a pose grammar model to encode the human body configuration of human poses from

2D space to 3D space. We follow this two-stage pipeline because pre-trained 2D pose estimators [4] are mature enough to be deployed elsewhere.

Video pose estimation. Since past and future frames are beneficial for 3D human pose estimation when the pose of a person is ambiguous or the body is partially occluded in one frame, many approaches tried to exploit temporal information [1, 31, 34, 41]. To predict temporally consistent 3D poses, Hossain *et al.* [34] designed a sequence-to-sequence network with LSTM. Pavllo *et al.* [31] introduced a fully convolutional model based on dilated temporal convolution. Cai *et al.* [1] directly chose the 3D pose of the target frame from outputs of the proposed graph-based method and then fed it to a refinement model. To produce smoother 3D sequences, Wang *et al.* [41] designed an U-shaped graph convolutional network and involved motion modeling into learning. However, this architecture is limit to embed fixed-length sequences. Different from most existing works that employed LSTM-based, graph-based, or fully convolutional architectures to exploit temporal information, we propose to leverage a Transformer-based architecture to capture long-range dependencies from input 2D pose sequences. Furthermore, compared to previous methods [1, 41] that either utilizing a refinement model or using a motion loss, we design a full-to-single supervision scheme to produce predictions at both the full sequence scale and single target frame scale rather than using a single component with a single output.

Transformer network. Transformer architecture was first proposed by [39] and commonly used in various language tasks. Recently, Transformer has shown promising performance in computer vision task, such as object detection [2, 48] and image classification [6, 45]. Unlike DETR [2] and ViT [6] that directly applied Transformer to images, we use Transformer to map 2D keypoints to 3D poses. Additionally, local context is incorporated into the standard Transformer to deal with the redundancy of sequences for the video-based 3D pose estimation task.

3. Lifting Transformer

Our proposed Lifting Transformer is illustrated in Figure 2. Given a sequence of the estimated 2D poses $P = \{p_1, \dots, p_T\}$ from videos, we aim to reconstruct 3D joint locations $X \in \mathbb{R}^{J \times 3}$ for a target frame, where $p_t \in \mathbb{R}^{J \times 2}$ denotes the 2D joint locations at frame t , T is the number of video frames, and J is the number of joints. The network contains a vanilla Transformer encoder (VTE) followed by a strided Transformer encoder (STE) and is trained in a full-to-single prediction scheme at both the full sequence scale and single target frame scale. Specifically, VTE is first used to model long-range information and is supervised by the full sequence scale to enforce temporal smoothness. Then, the information is aggregated in a global and local fashion

to one target pose representation from the proposed STE.

3.1. Transformer for 3D Pose Estimation

Motivated by the substantial performance gains achieved by the Transformer architecture in NLP, we propose to employ the Transformer encoder to solve the 3D human pose estimation. Each layer of the encoder has two sub-modules in [39]: a multi-head self-attention and a position-wise feed-forward network (FFN).

Multi-head attention. The core mechanism of Transformer is the multi-head self-attention. Specifically, suppose there are a set of queries (Q) and keys (K) of dimension d_k , and values (V) of dimension d_v , then a multi-head attention [39] can be computed as:

$$\text{MultiHead}(Q, K, V) = \text{Concat} (head_1, \dots, head_h) W^O,$$

$$head_i = \text{Self-Attn} \left(QW_i^Q, KW_i^K, VW_i^V \right), \quad (1)$$

where $\text{Self-Attn}(Q, K, V) = \text{softmax} \left(\frac{QK^T}{\sqrt{d_k}} \right) V$ and $W_i^Q \in \mathbb{R}^{d_m \times d_k}$, $W_i^K \in \mathbb{R}^{d_m \times d_k}$, $W_i^V \in \mathbb{R}^{d_m \times d_v}$, and $W^O \in \mathbb{R}^{hd_v \times d_m}$ are parameter matrices. The hyperparameters h is the number of multi-attention heads, d_m is the dimension of model, and $d_k = d_v = d_m/h$ in our implementation.

Feed-forward networks. In the existing FFN (formulation (2)) from VTE, it always maintains a full-length sequence of hidden representations across all layers. It contains significant redundancy for video-based pose estimation, as nearby poses are quite similar. However, to reconstruct more accurate 3D body joints of the target frame, crucial information should be extracted from the entire pose sequences. Therefore, it requires selectively aggregating the useful information.

To tackle this issue, inspired from the previous works [26, 31] that employ temporal convolutions to handle varying length sequences, we make modifications to the generic FFN. Given the input feature vector $x \in \mathbb{R}^{T \times C_{in}}$ with T sequences and C_{in} channels to generate an output of (\bar{T}, C_{out}) features, the operation performed by FFN can be computed as:

$$\text{FFN}_{t, c_{out}}(x) = \sum_i^{C_{in}} w_{c_{out}, i} * x_{t, i} \quad (2)$$

If 1D convolution is considered with kernel size K and strided factor S , a convolution feed-forward network can be computed as:

$$\text{CFFN}_{S(t), c_{out}}(x) = \sum_i^{C_{in}} \sum_k^K w_{c_{out}, i, k} * x_{S(t - \frac{K-1}{2} + k), i} \quad (3)$$

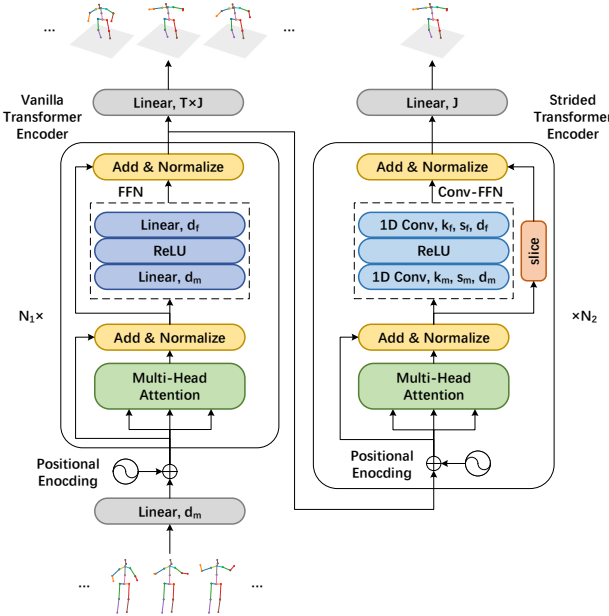


Figure 3. The network architecture of our proposed Lifting Transformer, where the left is VTE and the right is STE with strided convolutions that reconstructs the target 3D body joints by progressively reducing the sequence length. Here, N_1 and N_2 denotes the layers of the two modules, respectively. The hyperparameters k , s , d_m and d_f are the kernel size, the strided factor, the dimensions, and the number of hidden units. We slice the residuals to match the temporal dimensions of subsequent tensors.

Strided Transformer Encoder. In this way, fully-connected layers in FFN of VTE are replaced with strided convolutions. The modified VTE is termed as strided Transformer encoder (STE), which consists of a multi-head self-attention and a convolution feed-forward network, as presented in Figure 3 (right). STE is a global and local architecture, where self-attention mechanism models global context and strided convolution helps capture local context. It gradually reduces the temporal dimensionality from layer to layers to merge the nearby poses to a short sequence length representation. More importantly, the redundancy of all frames is reduced and hence boosts the model capacity.

3.2. Transformer-based Full-to-single Prediction

The iterative refinement scheme aimed at producing predictions in multiple processing stages is effective for 3D pose estimation [1, 30]. Inspired by the success of such iterative processing, we also consider a refinement scheme. Furthermore, we note that directly supervised the model at the single target frame scale always ignores temporal smoothness between video frames, while only supervised at a full sequence scale cannot explicitly learn a specific representation for the target frame.

To incorporate both scale constraints into the framework, a full-to-single scheme is proposed, which further refines

the intermediate predictions to produce more accurate estimations rather than using a single component with a single output. The first step is to supervise with full sequence scale by imposing extra temporal smoothness constraints during training from the outputs of VTE. A sequence loss \mathcal{L}_f is adopted to improve upon single frame predictions for temporal consistency over a sequence. This loss ensures that the estimated 3D poses from VTE coincide with the ground-truth 3D joint sequences:

$$\mathcal{L}_f = \sum_{t=1}^T \sum_{i=1}^J \left\| Y_i^t - \tilde{X}_i^t \right\|_2, \quad (4)$$

where \tilde{X}_i^t and Y_i^t represents the estimated 3D poses and ground truth 3D joint locations of joint i at frame t , respectively.

In the second step, the supervision is upon the output of STE, which is a progressive reduction architecture to reduce the temporal dimensionality from layer to layer. The output is a prediction of the 3D poses for all frames in the input sequences using both past and future data. A single-frame loss \mathcal{L}_s is used to minimize the distance between the estimated 3D poses X from STE and the target ground-truth 3D joint annotations Y :

$$\mathcal{L}_s = \sum_{i=1}^J \left\| Y_i - X_i \right\|_2. \quad (5)$$

In our implementation, the model is supervised at both the full sequence scale and single target frame scale. We train the entire network in an end-to-end manner with the combined loss:

$$\mathcal{L} = \lambda_f \mathcal{L}_f + \lambda_s \mathcal{L}_s, \quad (6)$$

where $\lambda_f = 1$ and $\lambda_s = 1$ are weighting factors.

4. Experiments and Discussions

4.1. Datasets and Evaluation

The proposed method is evaluated on two challenging benchmark datasets, i.e., Human3.6M [15] and HumanEva-I [35].

The Human3.6M dataset is the largest publicly available dataset for 3D human pose estimation, which consists of 3.6 million images captured from 4 synchronized 50Hz cameras. There are 7 professional subjects performing 15 everyday activities such as “Waiting”, “Smoking”, and “Posing”. Following the standard protocol in prior works [3, 38], 5 subjects (S1, S5, S6, S7, S8) are used for training and 2 subjects (S9 and S11) are used for evaluation. The frames from all views are trained by a single model for all actions. HumanEva-I is a much smaller dataset with fewer subjects and actions compared to Human3.6M. Following [18, 31],

Protocol #1	Dir.	Disc	Eat	Greet	Phone	Photo	Pose	Purch.	Sit	SitD.	Smoke	Wait	WalkD.	Walk	WalkT.	Avg.
Martinez <i>et al.</i> (ICCV'17) [27]	51.8	56.2	58.1	59.0	69.5	78.4	55.2	58.1	74.0	94.6	62.3	59.1	65.1	49.5	52.4	62.9
Fang <i>et al.</i> (AAAI'18) [7]	50.1	54.3	57.0	57.1	66.6	73.3	53.4	55.7	72.8	88.6	60.3	57.7	62.7	47.5	50.6	60.4
Zhao <i>et al.</i> (CVPR'19) [46]	47.3	60.7	51.4	60.5	61.1	49.9	47.3	68.1	86.2	55.0	67.8	61.0	42.1	60.6	45.3	57.6
Pavlakos <i>et al.</i> (CVPR'18) [29]	48.5	54.4	54.4	52.0	59.4	65.3	49.9	52.9	65.8	71.1	56.6	52.9	60.9	44.7	47.8	56.2
Lee <i>et al.</i> (ECCV'18) [18]	40.2	49.2	47.8	52.6	50.1	75.0	50.2	43.0	55.8	73.9	54.1	55.6	58.2	43.3	43.3	52.8
Liu <i>et al.</i> (ECCV'20) [23]	46.3	52.2	47.3	50.7	55.5	67.1	49.2	46.0	60.4	71.1	51.5	50.1	54.5	40.3	43.7	52.4
Cai <i>et al.</i> (ICCV'19) [1]	44.6	47.4	45.6	48.8	50.8	59.0	47.2	43.9	57.9	<u>61.9</u>	49.7	46.6	51.3	37.1	39.4	48.8
Pavllo <i>et al.</i> (CVPR'19) [31]	45.2	46.7	43.3	45.6	48.1	55.1	44.6	44.3	57.3	65.8	47.1	44.0	49.0	32.8	33.9	46.8
Xu <i>et al.</i> (CVPR'20) [44]	<u>37.4</u>	43.5	42.7	42.7	46.6	59.7	41.3	45.1	52.7	60.2	45.8	<u>43.1</u>	47.7	33.7	37.1	45.6
Liu <i>et al.</i> (CVPR'20) [26]	41.8	44.8	<u>41.1</u>	44.9	47.4	54.1	43.4	<u>42.2</u>	56.2	63.6	<u>45.3</u>	<u>45.3</u>	<u>31.3</u>	32.2	<u>45.1</u>	
Ours (T=243 CPN)	43.6	<u>44.2</u>	41.0	<u>43.8</u>	46.4	<u>52.7</u>	43.8	41.3	<u>56.1</u>	62.8	45.1	42.9	45.0	30.9	31.2	44.7
Protocol #2	Dir.	Disc	Eat	Greet	Phone	Photo	Pose	Purch.	Sit	SitD.	Smoke	Wait	WalkD.	Walk	WalkT.	Avg.
Martinez <i>et al.</i> (ICCV'17) [27]	39.5	43.2	46.4	47.0	51.0	56.0	41.4	40.6	56.5	69.4	49.2	45.0	49.5	38.0	43.1	47.7
Fang <i>et al.</i> (AAAI'18) [7]	38.2	41.7	43.7	44.9	48.5	55.3	40.2	38.2	54.5	64.4	47.2	44.3	47.3	36.7	41.7	45.7
Pavlakos <i>et al.</i> (CVPR'18) [29]	34.7	39.8	41.8	38.6	42.5	47.5	38.0	36.6	50.7	56.8	42.6	39.6	43.9	32.1	36.5	41.8
Liu <i>et al.</i> (ECCV'20) [23]	35.9	40.0	38.0	41.5	42.5	51.4	37.8	36.0	48.6	56.6	41.8	38.3	42.7	31.7	36.2	41.2
Cai <i>et al.</i> (ICCV'19) [1]	35.7	37.8	36.9	40.7	39.6	45.2	37.4	34.5	46.9	<u>50.1</u>	40.5	36.1	41.0	29.6	33.2	39.0
Pavllo <i>et al.</i> (CVPR'19) [31]	34.1	36.1	34.4	37.2	36.4	42.2	34.4	33.6	45.0	<u>52.5</u>	37.4	33.8	37.8	<u>25.6</u>	<u>27.3</u>	36.5
Xu <i>et al.</i> (CVPR'20) [44]	31.0	34.8	34.7	34.4	36.2	43.9	31.6	<u>33.5</u>	42.3	49.0	<u>37.1</u>	33.0	39.1	26.9	31.9	<u>36.2</u>
Ours (T=243 CPN)	<u>33.9</u>	<u>36.0</u>	34.3	<u>36.3</u>	36.8	41.9	34.8	32.6	<u>44.9</u>	52.5	37.0	34.1	36.5	24.7	26.1	36.1

Table 1. Quantitative comparisons with the state-of-the-art methods on Human3.6M under protocol #1 and protocol #2, where T denotes the number of input frames used. (CPN) - Cascaded Pyramid Network. Best in bold, second-best underlined.

Model	Parameters	MPJPE (mm)
Pavllo <i>et al.</i> [31] ($T = 27$)	8.56M	48.8
Pavllo <i>et al.</i> [31] ($T = 81$)	12.75M	47.7
Pavllo <i>et al.</i> [31] ($T = 243$)	16.95M	46.8
Liu <i>et al.</i> [26] ($T = 27$)	5.69M	48.5
Liu <i>et al.</i> [26] ($T = 81$)	8.46M	46.3
Liu <i>et al.</i> [26] ($T = 243$)	11.25M	45.1
Ours ($T = 27$)	3.22M	46.9
Ours ($T = 81$)	3.28M	45.9
Ours ($T = 243$)	3.44M	44.7

Table 2. Quantitative comparisons with state-of-the-art methods in different receptive fields on Human3.6M. The MPJPE metric and number of parameters are reported. Best in bold.

a single model is trained for all subjects (S1, S2, S3) and all actions (Walk, Jog, Box).

Two common evaluation protocols are used in the experiments. The mean per joint position error (MPJPE) is the average Euclidean distance between the ground-truth and predicted positions of the joints, which is referred to as protocol #1 in many works [7, 17]. Procrustes analysis MPJPE (P-MPJPE) is adopted, where the estimated 3D pose is aligned to the ground truth in translation, rotation, and scale, which is referred to as protocol #2 [27, 34].

4.2. Implementation Details

In our experiments, the input layer takes the concatenated (x, y) coordinates of the J joints for each frame and extracts sequence features using a linear layer. VTE [39] is adopted as the basic architecture. We choose encoder layers $N_1 = N_2 = 3$, multi-attention heads $h = 8$, dimensions

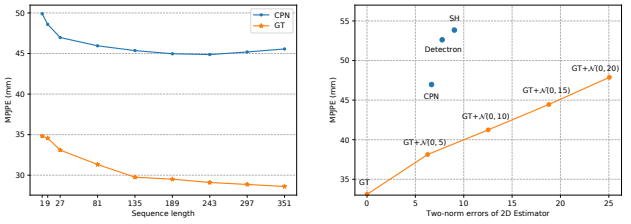


Figure 4. Left: ablation studies on different sequence lengths of our method on Human3.6M with the MPJPE metric. Right: the impact of 2D detections on Human3.6M. Here, $\mathcal{N}(0, \sigma^2)$ represents the Gaussian noise with mean zero and σ is the standard deviation. (CPN) - Cascaded Pyramid Network; (SH) Stack Hourglass; (GT) - 2D ground truth.

$d_m = 256$, and hidden units $d_f = 512$ for both VTE and STE. The kernel size and strided factor s_m are set to 1 in all STE layers. The strided factor s_f is set to $\{3, 3, 3\}$ for the receptive field of 27 frames, $\{3, 3, 9\}$ for 81, and $\{3, 9, 9\}$ for 243. The learnable position embeddings are used for the first layer of VTE and every layer of STE due to the different sequence lengths. Finally, we reproject the outputs via a linear layer. Note that we only use the outputs of STE as the final predictions for the full-to-single prediction scheme.

The 2D poses can be obtained by performing any classic 2D pose detections or directly using the 2D ground truth. Following [31], the cascaded pyramid network (CPN) [4] is used for Human3.6M and Mask R-CNN [13] is adopted for HumanEva-I to obtain 2D poses for a fair comparison.

In this work, all experiments are conducted on the PyTorch framework with one GeForce GTX 3090 GPU. The network is trained using Adam optimizer with a mini-batch

Protocol #1	Dir.	Disc	Eat	Greet	Phone	Photo	Pose	Purch.	Sit	SitD.	Smoke	Wait	WalkD.	Walk	WalkT.	Avg.
Martinez <i>et al.</i> (ICCV'17)[27]	37.7	44.4	40.3	42.1	48.2	54.9	44.4	42.1	54.6	58.0	45.1	46.4	47.6	36.4	40.4	45.5
Lee <i>et al.</i> (ECCV'18) [18]	<u>32.1</u>	<u>36.6</u>	34.3	37.8	44.5	49.9	40.9	36.2	44.1	45.6	35.3	35.9	<u>30.3</u>	37.6	35.5	38.4
Pavllo <i>et al.</i> (CVPR'19) [31]	35.2	40.2	<u>32.7</u>	35.7	38.2	45.5	40.6	36.1	48.8	47.3	37.8	39.7	38.7	27.8	29.5	37.8
Cai <i>et al.</i> (ICCV'19) [1]	32.9	38.7	32.9	37.0	37.3	44.8	<u>38.7</u>	36.1	41.0	45.6	36.8	37.7	37.7	29.5	31.6	37.2
Liu <i>et al.</i> (CVPR'20) [26]	34.5	37.1	33.6	<u>34.2</u>	<u>32.9</u>	<u>37.1</u>	39.6	<u>35.8</u>	<u>40.7</u>	41.4	<u>33.0</u>	<u>33.8</u>	33.0	<u>26.6</u>	<u>26.9</u>	34.7
Wang <i>et al.</i> (ECCV'20) (†) [41]	-	-	-	-	-	-	-	-	-	-	-	-	-	-	<u>32.0</u>	
Ours (T=243 GT)	26.9	30.6	27.2	27.4	29.7	33.6	31.9	26.3	37.8	38.6	29.0	29.2	27.5	19.8	20.3	29.1

Table 3. Quantitative comparisons of MPJPE in millimeter on Human3.6M under protocol #1, using ground truth 2D joint locations as input. Best in bold, second-best underlined. (†) - To ensure fair comparison with our method, we report the version without motion loss.

	Walk			Jog			Box			Avg.
	S1	S2	S3	S1	S2	S3	S1	S2	S3	
Martinez <i>et al.</i> [27]	19.7	17.4	46.8	26.9	18.2	18.6	-	-	-	-
Pavlakos <i>et al.</i> [30]	22.3	19.5	29.7	28.9	21.9	23.8	-	-	-	-
Lee <i>et al.</i> [18]	18.6	19.9	<u>30.5</u>	25.7	16.8	17.7	42.8	48.1	53.4	30.3
Pavllo <i>et al.</i> [31]	13.9	<u>10.2</u>	46.6	<u>20.9</u>	13.1	13.8	23.8	<u>33.7</u>	<u>32.0</u>	<u>23.1</u>
Ours (T=27 MRCNN)	14.0	10.0	32.8	19.5	<u>13.6</u>	<u>14.2</u>	22.4	21.6	22.5	18.9
Ours (T=27 GT)	9.7	7.6	15.8	12.3	9.4	11.2	14.8	12.9	16.5	12.2

Table 4. Quantitative results on HumanEva-I dataset under protocol #2. Best in bold, second-best underlined. (MRCNN) - Mask-RCNN; (GT) - 2D ground truth.

size of 256 for Human3.6M, 64 for HumanEva-I. An initial learning rate of 0.001 is used with a shrink factor of 0.95 applied after each epoch and 0.5 after every 5 epochs. Note that we only adopt horizontal flip augmentation during training and test stages and only compute MPJPE loss for training.

4.3. Comparison with the State-of-the-art

We compare our method with the previous state-of-the-art approaches on Human3.6M dataset. As shown in Table 1, the performance of our 243-frame model with CPN input is presented. Our method outperforms the state-of-the-art methods on Human3.6 under all metrics (44.7 mm on protocol #1 and 36.1 mm on protocol #2).

Table 2 compares the MPJPE metric and number of parameters with several state-of-the-art methods in different receptive fields ($T = 27, 81, 243$) on Human3.6M. It can be seen that our method has the fewest parameters but achieves the best performance from overall receptive fields. This shows that our proposed Transformer-based network is more efficient than fully convolutional architectures at the same level of accuracy for video 3D pose estimation. Besides, our model is lightweight and parameters hardly increase with the increased receptive fields, which is practical for real-time applications. Figure 5 shows the visualized qualitative results from the 243-frame models of TCN [31], ATTN-TCN [26], and our model.

Additionally, we report the results when using ground truth 2D poses to explore the upper bound of our method. As illustrated in Table 3, it can be seen that our method achieves the best result (29.1 mm in MPJPE) outperforming all other methods. Moreover, it has a larger performance gain than CPN input compared with state-of-the-art meth-

ods, which indicates that our method has a stronger capacity in capturing temporal dependencies from more accurate 2D representations.

To evaluate the generalizability of our model to smaller datasets, experiments are conducted on HumanEva-I based on Mask R-CNN 2D detections and 2D ground truth. The results are given in Table 4, which demonstrates that our method achieves promising results in each action.

4.4. Ablation Studies

Input sequence length. The MPJPE results of our model with different sequence lengths on Human3.6M are shown in Figure 4 (left). It can be seen that with more input frames used for predictions, our proposed method obtains larger gains when using ground truth 2D poses. This is expected since direct lifting 3D poses from disjointed 2D poses leads to temporally incoherent outputs [5]. Particularly the best results are obtained with $T = 243$ (44.7 mm) by using CPN. However, the performance decreases when $T = 297$ (45.1 mm) and $T = 351$ (45.5 mm), which is the same phenomenon as [26]. The reason is that the 2D detector CPN is limited to provide useful information for our model to distinguish the discriminative representation from redundant long sequences. Next, we choose $T = 27$ on Human3.6M in the following ablation experiments as a compromise between the accuracy and the computational complexity.

2D detections. For the 2D-3D lifting task, the accuracy of the 2D detections directly influences the results of 3D pose estimation [27]. To show the effectiveness of our method on different 2D pose detectors, we carry out experiments with the detections from Stack Hourglass (SH) [28], Detectron [31], and CPN [4]. Moreover, to test the tolerance of our method to different levels of noise, we also train our network by 2D ground truth (GT) with different levels of additive Gaussian noises. The results are shown in Figure 4 (right). It can be observed that the MPJPE of 3D poses increases linearly with the two-norm errors of 2D poses. Note that 2D pose detector methods achieve worse estimation performance than 2D ground truth with noises, which is due to the self-occlusions problem for 2D pose estimation.

Model hyperparameters. As shown in Table 5, we

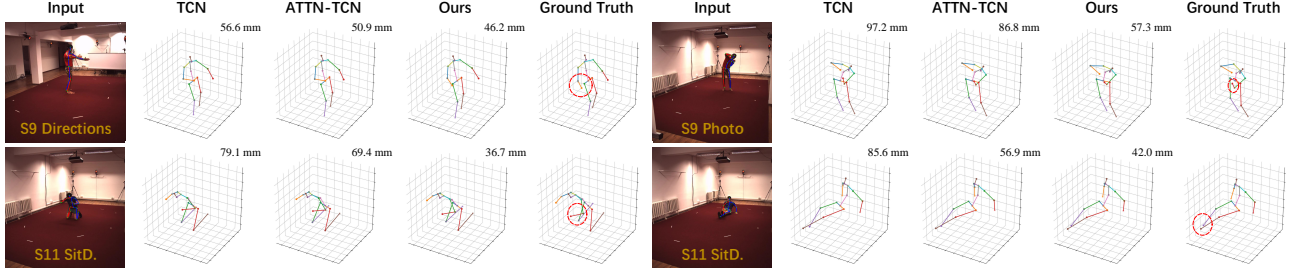


Figure 5. Qualitative comparisons with the previous state-of-the-art methods, 243-frame model of TCN [31] and ATTN-TCN [26] on Human3.6M dataset.

N_1	N_2	d_m	d_f	Parameters	FLOPs	MPJPE (mm)
2	-	512	2048	6.36M	171.08M	47.9
3	-	512	2048	9.51M	256.02M	47.8
4	-	512	2048	12.66M	340.95M	48.1
5	-	512	2048	15.82M	425.89M	48.4
6	-	512	2048	18.97M	510.82M	48.6
2	-	256	512	1.08M	28.92M	47.8
3	-	256	512	1.61M	43.07M	47.5
4	-	256	512	2.13M	57.23M	47.9
5	-	256	512	2.66M	71.38M	47.8
6	-	256	512	3.19M	85.54M	47.9
-	3	256	512	1.61M	17.68M	48.3
2	3	256	512	2.69M	45.99M	47.4
3	3	256	512	3.22M	60.15M	46.9
2	3	512	2048	15.89M	266.62M	47.7
3	3	512	2048	19.04M	351.55M	48.1

Table 5. Ablation study on the hyperparameters of our model on Human3.6M under protocol #1. N_1 and N_2 is the number of VTE and STE layers, respectively. d_m and d_f are the dimensions and the number of hidden units.

first analyze the effect of the number of VTE layers. Empirically, it can be found that the performance cannot be improved when naively stacking multiple standard Transformer encoder layers. However, our model that introduces STE is more accurate at the same level of the number of Transformer encoder layers and model parameters. For example, our method ($N_1 = 3$ and $N_2 = 3$) has better performance and fewer FLOPs than $N_1 = 6$ at the same $d_m = 256$ and $d_f = 512$ hidden units (46.9 mm vs. 47.9 mm, 60.15M vs. 85.54M). Meanwhile, our STE ($N_2 = 3$, 17.68M) also have fewer FLOPs than standard Transformer encoder ($N_1 = 3$, 43.07M) with similar parameters, which achieves $2.4 \times$ less computation. It verifies the effectiveness of our proposed STE that merges the nearby poses to reduce the redundancy of the sequence in a simple form. Then, we investigate the hyperparameters on the performance and parameters of both modules. It can be observed that using 3 encoder layers, 256 dimensions, and 512 hidden units achieves the best performance.

Strided factor. We also explore the design choice of

Layers	Strided factor	MPJPE (mm)	Δ
3	3, 3, 3	46.9	-
3	3, 9, 1	47.3	0.4
3	9, 3, 1	47.4	0.5
2	3, 9	47.4	0.5
2	9, 3	47.5	0.6
1	27	47.6	0.7

Table 6. Ablation study on the strided factor of STE with the receptive field $T = 3 \times 3 \times 3 = 27$. The evaluation is performed on Human3.6M under protocol #1.

Method	MPJPE (mm)	Δ
Ours, proposed	46.9	-
Ours, intermediate predictions	48.8	1.9
Ours, Pooling Transformer	47.3	0.4
w/o sequence loss	48.9	2.0
w/o VTE	48.3	1.4
w/o STE	47.5	0.6

Table 7. Ablation study on each component of our network architecture on Human3.6M under protocol #1.

strided factor for STE when fixing VTE with 3 encoder layers and 8 multi-attention heads, 256 dimensions, and 512 hidden units for both VTE and STE. The experimental results have been depicted in Table 6, it shows that using a strided factor $s_f = \{3, 3, 3\}$ has the best performance. It demonstrates the benefit of leveraging a progressive reduction architecture to gradually reduce the temporal dimensionality from layer to layer with a small strided factor.

Model components. An ablation study is performed to assess the effectiveness of different components of our method. As shown in Table 7, we select the center frames of the intermediate predictions from VTE as the final results, the MPJPE decreases by 1.9 mm (from 46.9 mm to 48.8 mm). Additionally, the sequence loss \mathcal{L}_f leads to a significant performance gain (2.0 mm). The empirical results indicate that the intermediate supervision allows for a stronger capacity in producing smooth 3D sequences. Following [49], we perform pooling operation after FFN of VTE and then replace STE of our proposed model with it,

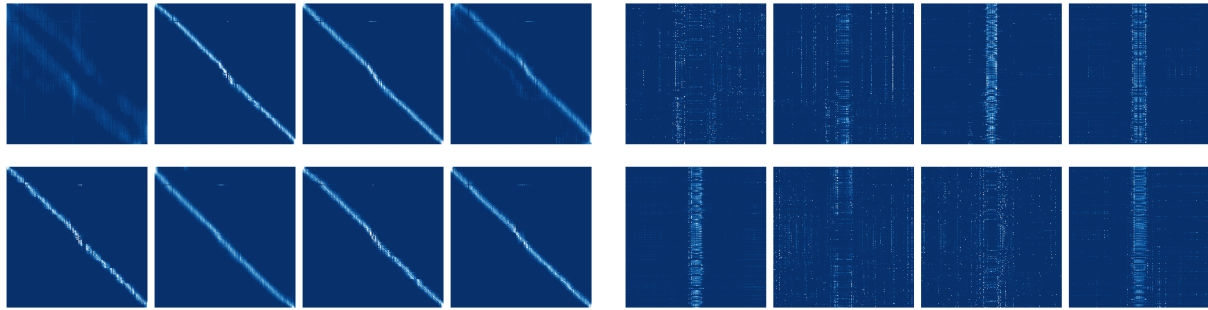


Figure 6. Multi-head attention maps ($h = 8$) from VTE (left) and STE (right) of our 243-frame model. It illustrates the self-attention mechanism systematically assigns a weight distribution to frames, all of which might contribute to the inference. The brighter color indicates stronger attention across frames.

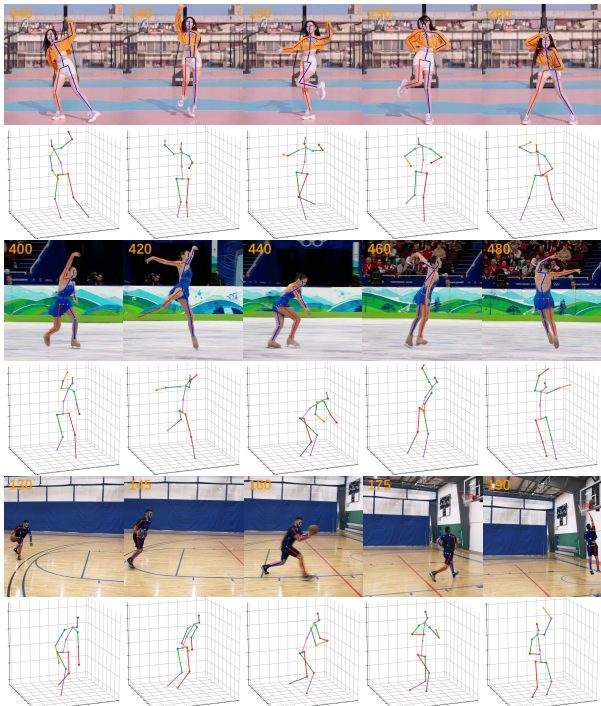


Figure 7. Qualitative results on challenging wild videos. The number is the frame index of input videos.

the new architecture is termed as Pooing Transformer. The error increases by 0.4 mm, which highlights that our STE can preserve more valuable information. Removing VTE (only trained with single-frame loss) leads to 1.4 mm increase in MPJPE error. Meanwhile, removing STE (only trained with sequence loss), the performance decreases. These results validate the effectiveness of our proposed full-to-single mechanism by using further processing to produce more accurate predictions.

4.5. Qualitative Results

Attention visualization. Our method is easily interpretable through visualizing the attention score across

frames to explain what temporal dependencies the target frame relies on. Visualization results of the multi-head attention maps of the first attention layers from VTE and STE (243-frame model) are shown in Figure 6. The left map shows it selectively identifies important sequences close to the input frames [16, 43] and the right map mainly pays strong attention to the target frame across all the sequences. This is expected since the proposed full-to-single strategy enables the VTE and STE modules to learn different representations, where VTE models long-range dependencies and enforces temporal consistency across frames, and STE learns a specific representation to reach an optimal inference for the target frame. Note that few attention head maps are sparse due to the different temporal patterns or semantics.

3D reconstruction visualization. We further evaluate our method on wild videos from YouTube, as shown in Figure 7. Despite the challenging samples with huge movements and hard actions, our model can produce realistic and structurally plausible 3D predictions from complicated pose articulation. This demonstrates that our method is robust to partial occlusions and tolerant to depth ambiguity. More results can be seen in the appendix.

5. Conclusion

We present Lifting Transformer network with strided Transformer encoder (STE) and full-to-single supervision scheme for lifting a sequence of 2D joint locations to a 3D pose. Compared with standard Transformer encoder, the proposed STE can aggregate long-range information to a single-vector pose in a global and local fashion. Meanwhile, the computation cost can be reduced by a large margin. The proposed full-to-single supervision scheme enforces temporal smoothness and further refines the estimation. Comprehensive experiments on two benchmark datasets demonstrate that our method achieves superior performance compared to state-of-the-art methods.

References

[1] Yujun Cai, Liuhan Ge, Jun Liu, Jianfei Cai, Tat-Jen Cham, Junsong Yuan, and Nadia Magnenat Thalmann. Exploiting spatial-temporal relationships for 3d pose estimation via graph convolutional networks. In *Proceedings of the IEEE International Conference on Computer Vision (ICCV)*, pages 2272–2281, 2019. 1, 3, 4, 5, 6, 11

[2] Nicolas Carion, Francisco Massa, Gabriel Synnaeve, Nicolas Usunier, Alexander Kirillov, and Sergey Zagoruyko. End-to-end object detection with transformers. In *European Conference on Computer Vision (ECCV)*, pages 213–229. Springer, 2020. 3

[3] Xipeng Chen, Kwan-Yee Lin, Wentao Liu, Chen Qian, and Liang Lin. Weakly-supervised discovery of geometry-aware representation for 3d human pose estimation. In *Proceedings of the IEEE Conference on Computer Vision and Pattern Recognition (CVPR)*, pages 10895–10904, 2019. 4

[4] Yilun Chen, Zhicheng Wang, Yuxiang Peng, Zhiqiang Zhang, Gang Yu, and Jian Sun. Cascaded pyramid network for multi-person pose estimation. In *Proceedings of the IEEE Conference on Computer Vision and Pattern Recognition (CVPR)*, pages 7103–7112, 2018. 3, 5, 6

[5] Rishabh Dabral, Anurag Mundhada, Uday Kusupati, Safeer Afaque, Abhishek Sharma, and Arjun Jain. Learning 3d human pose from structure and motion. In *Proceedings of the European Conference on Computer Vision (ECCV)*, pages 668–683, 2018. 1, 6

[6] Alexey Dosovitskiy, Lucas Beyer, Alexander Kolesnikov, Dirk Weissenborn, Xiaohua Zhai, Thomas Unterthiner, Mostafa Dehghani, Matthias Minderer, Georg Heigold, Sylvain Gelly, et al. An image is worth 16x16 words: Transformers for image recognition at scale. *arXiv preprint arXiv:2010.11929*, 2020. 3

[7] Hao-Shu Fang, Yuanlu Xu, Wenguan Wang, Xiaobai Liu, and Song-Chun Zhu. Learning pose grammar to encode human body configuration for 3d pose estimation. In *Thirty-Second AAAI Conference on Artificial Intelligence*, 2018. 2, 5

[8] Mercedes Garcia-Salguero, Javier Gonzalez-Jimenez, and Francisco-Angel Moreno. Human 3d pose estimation with a tilting camera for social mobile robot interaction. *Sensors*, 19(22):4943, 2019. 1

[9] Mor Geva, Roei Schuster, Jonathan Berant, and Omer Levy. Transformer feed-forward layers are key-value memories. *arXiv preprint arXiv:2012.14913*, 2020. 2

[10] Liang-Yan Gui, Kevin Zhang, Yu-Xiong Wang, Xiaodan Liang, José MF Moura, and Manuela Veloso. Teaching robots to predict human motion. In *Proceedings of the IEEE/RSJ International Conference on Intelligent Robots and Systems (IROS)*, pages 562–567, 2018. 1

[11] Kai Han, Yunhe Wang, Hanting Chen, Xinghao Chen, Jianyuan Guo, Zhenhua Liu, Yehui Tang, An Xiao, Chunjing Xu, Yixing Xu, et al. A survey on visual transformer. *arXiv preprint arXiv:2012.12556*, 2020. 2

[12] Liang Han, Pichao Wang, Zhaozheng Yin, Fan Wang, and Hao Li. Exploiting better feature aggregation for video object detection. In *Proceedings of the 28th ACM International Conference on Multimedia*, pages 1469–1477, 2020. 2

[13] Kaiming He, Georgia Gkioxari, Piotr Dollár, and Ross Girshick. Mask r-cnn. In *Proceedings of the IEEE international conference on computer vision (ICCV)*, pages 2961–2969, 2017. 5

[14] Shuteng He, Hao Luo, Pichao Wang, Fan Wang, Hao Li, and Wei Jiang. Transreid: Transformer-based object re-identification. *arXiv preprint arXiv:2102.04378*, 2021. 2

[15] Catalin Ionescu, Dragos Papava, Vlad Olaru, and Cristian Sminchisescu. Human3.6m: Large scale datasets and predictive methods for 3d human sensing in natural environments. *IEEE Transactions on Pattern Analysis and Machine Intelligence*, 36(7):1325–1339, 2013. 2, 4

[16] Zihang Jiang, Weihao Yu, Daquan Zhou, Yunpeng Chen, Jiashi Feng, and Shuicheng Yan. Convbert: Improving bert with span-based dynamic convolution. In *Advances in Neural Information Processing Systems (NIPS)*, 2020. 8

[17] Muhammed Kocabas, Salih Karagoz, and Emre Akbas. Self-supervised learning of 3d human pose using multi-view geometry. In *Proceedings of the IEEE Conference on Computer Vision and Pattern Recognition (CVPR)*, pages 1077–1086, 2019. 5

[18] Kyoungoh Lee, Inwoong Lee, and Sanghoon Lee. Propagating lstm: 3d pose estimation based on joint interdependency. In *Proceedings of the European Conference on Computer Vision (ECCV)*, pages 119–135, 2018. 1, 4, 5, 6

[19] Sijin Li and Antoni B Chan. 3d human pose estimation from monocular images with deep convolutional neural network. In *Asian Conference on Computer Vision (ACCV)*, pages 332–347, 2014. 1

[20] Xiangyu Li, Yonghong Hou, Pichao Wang, Zhimin Gao, Mingliang Xu, and Wanqing Li. Trear: Transformer-based rgb-d egocentric action recognition. *arXiv preprint arXiv:2101.03904*. 2

[21] Xiangyu Li, Yonghong Hou, Pichao Wang, Zhimin Gao, Mingliang Xu, and Wanqing Li. Transformer guided geometry model for flow-based unsupervised visual odometry. *Neural Computing and Applications*, pages 1–12, 2021. 2

[22] Jun Liu, Henghui Ding, Amir Shahroudy, Ling-Yu Duan, Xudong Jiang, Gang Wang, and Alex C Kot. Feature boosting network for 3d pose estimation. *IEEE Transactions on Pattern Analysis and Machine Intelligence*, 42(2):494–501, 2019. 2

[23] Kenkun Liu, Rongqi Ding, Zhiming Zou, Le Wang, and Wei Tang. A comprehensive study of weight sharing in graph networks for 3d human pose estimation. In *Proceedings of the European Conference on Computer Vision (ECCV)*, pages 318–334. Springer, 2020. 5

[24] Mengyuan Liu, Hong Liu, and Chen Chen. Enhanced skeleton visualization for view invariant human action recognition. *Pattern Recognition*, 68:346–362, 2017. 1

[25] Mengyuan Liu and Junsong Yuan. Recognizing human actions as the evolution of pose estimation maps. In *Proceedings of the IEEE Conference on Computer Vision and Pattern Recognition (CVPR)*, pages 1159–1168, 2018. 1

[26] Ruiyu Liu, Ju Shen, He Wang, Chen Chen, Sen-ching Cheung, and Vijayan Asari. Attention mechanism exploits temporal contexts: Real-time 3d human pose reconstruction. In *Proceedings of the IEEE Conference on Computer Vision and Pattern Recognition (CVPR)*, pages 5064–5073, 2020.

[2](#), [3](#), [5](#), [6](#), [7](#), [11](#)

[27] Julieta Martinez, Rayat Hossain, Javier Romero, and James J Little. A simple yet effective baseline for 3d human pose estimation. In *Proceedings of the IEEE International Conference on Computer Vision (ICCV)*, pages 2640–2649, 2017. [1](#), [2](#), [5](#), [6](#)

[28] Alejandro Newell, Kaiyu Yang, and Jia Deng. Stacked hourglass networks for human pose estimation. In *Proceedings of the European Conference on Computer Vision (ECCV)*, pages 483–499, 2016. [6](#)

[29] Georgios Pavlakos, Xiaowei Zhou, and Kostas Daniilidis. Ordinal depth supervision for 3d human pose estimation. In *Proceedings of the IEEE Conference on Computer Vision and Pattern Recognition (CVPR)*, pages 7307–7316, 2018. [5](#)

[30] Georgios Pavlakos, Xiaowei Zhou, Konstantinos G Derpanis, and Kostas Daniilidis. Coarse-to-fine volumetric prediction for single-image 3d human pose. In *Proceedings of the IEEE Conference on Computer Vision and Pattern Recognition (CVPR)*, pages 7025–7034, 2017. [2](#), [4](#), [6](#)

[31] Dario Pavllo, Christoph Feichtenhofer, David Grangier, and Michael Auli. 3d human pose estimation in video with temporal convolutions and semi-supervised training. In *Proceedings of the IEEE Conference on Computer Vision and Pattern Recognition (CVPR)*, pages 7753–7762, 2019. [1](#), [2](#), [3](#), [4](#), [5](#), [6](#), [7](#), [11](#)

[32] Katherine Pullen and Christoph Bregler. Motion capture assisted animation: Texturing and synthesis. In *Proceedings of the 29th annual conference on Computer graphics and interactive techniques*, pages 501–508, 2002. [1](#)

[33] Ibrahim Radwan, Abhinav Dhall, and Roland Goecke. Monocular image 3d human pose estimation under self-occlusion. In *Proceedings of the IEEE International Conference on Computer Vision (ICCV)*, pages 1888–1895, 2013. [1](#)

[34] Mir Rayat Imtiaz Hossain and James J Little. Exploiting temporal information for 3d human pose estimation. In *Proceedings of the European Conference on Computer Vision (ECCV)*, pages 68–84, 2018. [1](#), [3](#), [5](#)

[35] Leonid Sigal, Alexandru O Balan, and Michael J Black. HumanEva: Synchronized video and motion capture dataset and baseline algorithm for evaluation of articulated human motion. *International Journal of Computer Vision*, 87(1-2):4, 2010. [2](#), [4](#)

[36] Xiao Sun, Bin Xiao, Fangyin Wei, Shuang Liang, and Yichen Wei. Integral human pose regression. In *Proceedings of the European Conference on Computer Vision (ECCV)*, pages 529–545, 2018. [2](#)

[37] Yi Tay, Mostafa Dehghani, Dara Bahri, and Donald Metzler. Efficient transformers: A survey. *arXiv preprint arXiv:2009.06732*, 2020. [2](#)

[38] Denis Tome, Matteo Toso, Lourdes Agapito, and Chris Russell. Rethinking pose in 3d: Multi-stage refinement and recovery for markerless motion capture. In *2018 International Conference on 3D Vision (3DV)*, pages 474–483, 2018. [4](#)

[39] Ashish Vaswani, Noam Shazeer, Niki Parmar, Jakob Uszkoreit, Llion Jones, Aidan N Gomez, Łukasz Kaiser, and Illia Polosukhin. Attention is all you need. In *Advances in Neural Information Processing Systems (NIPS)*, pages 5998–6008, 2017. [1](#), [2](#), [3](#), [5](#)

[40] Bastian Wandt and Bodo Rosenhahn. Repnet: Weakly supervised training of an adversarial reprojection network for 3d human pose estimation. In *Proceedings of the IEEE Conference on Computer Vision and Pattern Recognition (CVPR)*, pages 7782–7791, 2019. [2](#)

[41] Jingbo Wang, Sijie Yan, Yuanjun Xiong, and Dahua Lin. Motion guided 3d pose estimation from videos. *arXiv preprint arXiv:2004.13985*, 2020. [1](#), [3](#), [6](#)

[42] Pichao Wang, Wanqing Li, Philip Ogunbona, Jun Wan, and Sergio Escalera. Rgb-d-based human motion recognition with deep learning: A survey. *Computer Vision and Image Understanding*, 171:118–139, 2018. [1](#)

[43] Zhanghao Wu, Zhijian Liu, Ji Lin, Yujun Lin, and Song Han. Lite transformer with long-short range attention. In *International Conference on Learning Representations (ICLR)*, 2020. [8](#)

[44] Jingwei Xu, Zhenbo Yu, Bingbing Ni, Jiancheng Yang, Xiaokang Yang, and Wenjun Zhang. Deep kinematics analysis for monocular 3d human pose estimation. In *Proceedings of the IEEE Conference on Computer Vision and Pattern Recognition (CVPR)*, pages 899–908, 2020. [5](#)

[45] Li Yuan, Yunpeng Chen, Tao Wang, Weihao Yu, Yujun Shi, Francis EH Tay, Jiashi Feng, and Shuicheng Yan. Tokens-to-token vit: Training vision transformers from scratch on imagenet. *arXiv preprint arXiv:2101.11986*, 2021. [3](#)

[46] Long Zhao, Xi Peng, Yu Tian, Mubbasis Kapadia, and Dimitris N Metaxas. Semantic graph convolutional networks for 3d human pose regression. In *Proceedings of the IEEE Conference on Computer Vision and Pattern Recognition (CVPR)*, pages 3425–3435, 2019. [2](#), [5](#)

[47] Xingyi Zhou, Qixing Huang, Xiao Sun, Xiangyang Xue, and Yichen Wei. Towards 3d human pose estimation in the wild: a weakly-supervised approach. In *Proceedings of the IEEE International Conference on Computer Vision (ICCV)*, pages 398–407, 2017. [1](#)

[48] Xizhou Zhu, Weijie Su, Lewei Lu, Bin Li, Xiaogang Wang, and Jifeng Dai. Deformable detr: Deformable transformers for end-to-end object detection. *arXiv preprint arXiv:2010.04159*, 2020. [3](#)

[49] Dai Zihang, Lai Guokun, Yang Yiming, and Quoc Le V. Funnel-transformer: Filtering out sequential redundancy for efficient language processing. In *Advances in Neural Information Processing Systems (NIPS)*, 2020. [2](#), [7](#)

6. Appendix

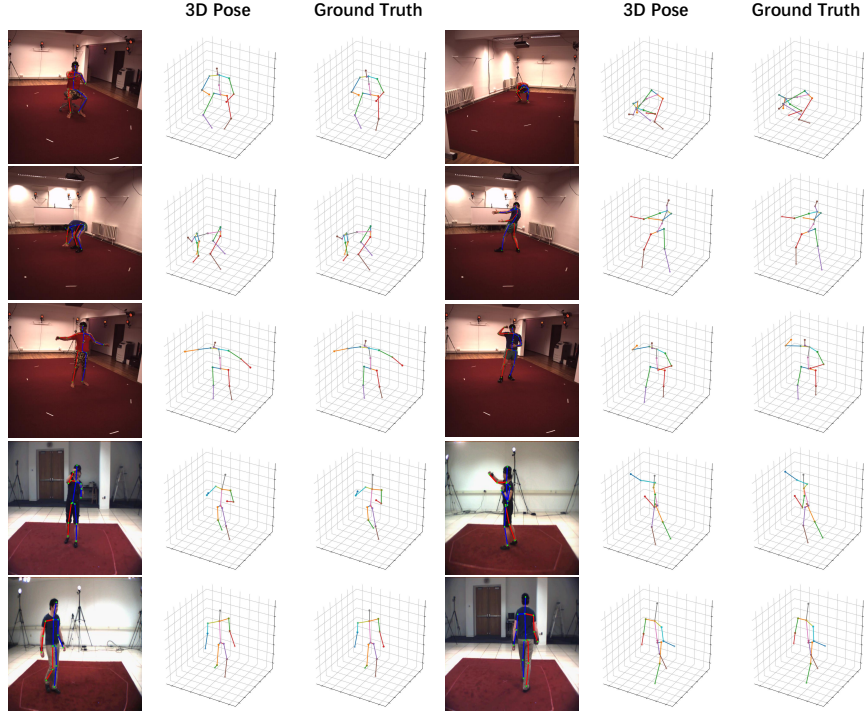


Figure 8. Visual results of our proposed method on Human3.6M dataset (first 3 rows) and HumanEva-I dataset (last 2 rows).

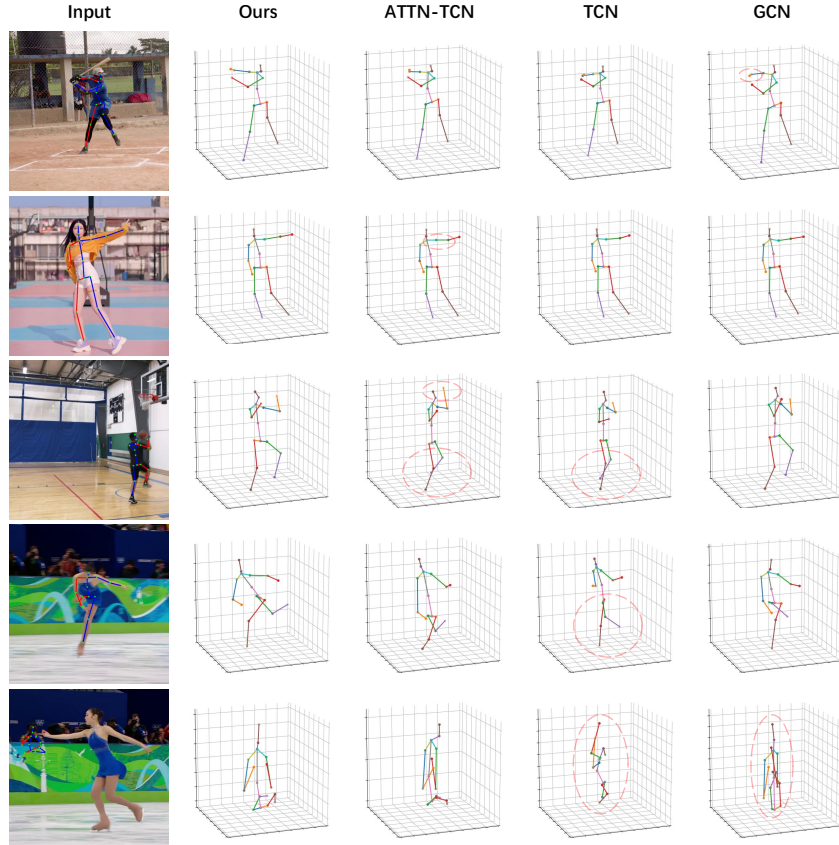


Figure 9. Qualitative comparisons on challenging in-the-wild videos with previous state-of-the-art methods, ATTN-TCN [26], TCN [31], and GCN [1] on Human3.6M dataset. The last row shows the failure case, where the 2D detector has failed badly.